Nonlinear Mitigation of a 400G Frequency-Hybrid Superchannel for the 62.5 GHz Slot

Sofia B. Amado, Fernando P. Guiomar, Nelson J. Muga, Antonino Nespola, Luca Bertignono, Andrea Carena and Armando N. Pinto

***Abstract*—We propose a 400G frequency-hybrid superchannel solution based on three carriers, two edge PM-16QAM and a central PM-64QAM carrier, compatible with the 62.5 GHz grid slot (spectral efficiency of 6.4 b/s/Hz). The proposed superchannel is experimentally assessed in long-haul transmission by co-propagation with other 8 similar superchannels. The optimum power-ratio between superchannel carriers is analytically determined in linear and nonlinear operation regimes using the enhanced Gaussian noise (EGN) model and validated by experimental and simulation results. The 400G superchannel performance is evaluated in terms of maximum reach determining the optimum launch power and considering three distinct forward-error correction (FEC) paradigms: superchannel FEC (SC-FEC) where a single FEC is applied to the entire superchannel, independent carrier FEC (IC-FEC) where an independent FEC with fixed overhead is applied to each superchannel carrier, and independent carrier flexible FEC (Flex-FEC) where optimized FEC overheads are applied independently to each superchannel carrier with the constraint of a given total overhead. When compared to the IC-FEC approach, the SC-FEC or Flex-FEC approaches enables to extend the maximum transmission distance by more than 60%, while reducing the optimum power-ratio by ∼6 dB, at the cost of 2 dB higher launched power. The system performance is also analyzed for the case of nonlinear compensation via digital backpropagation (DBP) techniques, assessing the improvement in reach and evaluating their impact on the optimum power-ratio and launch power. For the proposed frequency-hybrid superchannel, we demonstrate that the application of DBP can be restricted to the carrier with higher QAM cardinality, thereby significantly reducing the overall computational effort, with a maximum reach reduction of only ∼2% over the application of DBP to all three carriers individually.**

***Index Terms*—optical communication systems, digital signal processing, superchannels, digital backpropagation, 400G.**

I. Introduction

THE continuous growth of data traffic has been pushing the current 100G networks to its limits. Telecom operators look now for new cost-effective solutions for the next-generation optical transmission systems [1]–[3].

Optical systems based on superchannels and flexible networks have been attracting significant attention, due to their capability to increase the channel data-rate, spectral efficiency (SE) and adaptability to the traffic demand, while avoiding the replacement of the installed equipment [4]–[13]. Several enabling techniques have been recently proposed to add bit-rate granularity to networks, with emphasis for time-domain hybrid modulation formats (TDHMF) which have been intensively studied in several simulation and experimental works [14]–[17]. More recently, probabilistic constellation shaping has been proposed as an alternative solution for the increase of the bit-rate granularity in flexible networks, while shrinking the gap to Shannon capacity [18]–[20]. Although the same digital signal processing (DSP) algorithms can be used for the signal equalization at different spectral efficiencies, the coding and decoding subsystems tends to bring some additional complexity due to the required shaping [18]–[20].

The design of hybrid modulation optical systems involves a new key degree of freedom – the power-ratio (PR) between formats – which also depends on the transmitter operation strategy. In [21] four transmitter operation strategies for time-hybrid modulation formats were proposed and the respective theoretical optimum PR were derived for additive white Gaussian noise (AWGN) channels. However, the nonlinear effects generated during signal propagation in fiber may substantially change the optimum PR regimes derived for AWGN channels. An extended analysis of this issue requires the use of advanced nonlinear modeling techniques, such as the recently proposed enhanced Gaussian noise (EGN) model [22], which allows to take into account the impact of different modulation formats on the generated nonlinear interference (NLI).

Several 400G superchannel solutions based on dual- and triple-carrier PM-16QAM over 75 GHz (SE = 5.33 b/s/Hz) grid [11], [23]–[25] and triple-carrier PM-64QAM distributed over 50 GHz (SE = 8 b/s/Hz) grid [23] were previously proposed. These solutions proved to be suitable for ultra-long-haul (> 5000 km) and metro (< 1000 km) applications, respectively. However, there is this gap of distance (from 1000 km to 5000 km) for which other solutions might also be proposed. Moreover, given the recently standardized flexible grid of 12.5 GHz, solutions for the 62.5 GHz slot must also be developed, aiming to achieve a better tradeoff between SE and transmission distance. Possible superchannel solutions to be implemented under such conditions could resort on the use of PM-32QAM carriers. Although, due to

This work was supported in part by Fundação para a Ciência e a Tecnologia (FCT) through national funds under, and when applicable co-funded by FEDER - PT2020 partnership agreement, under the project UID/EEA/50008/2013 (actions SoftTransceiver and Optical-5G), and also by the Ph.D. grant PD/BD/52593/2014 and by the European Comission through a Marie Skłodowska-Curie individual fellowship, project Flex-ON (653412). The authors acknowledge Synopsys Inc. for providing the OptSim simulator.

S. B. Amado, N. J. Muga, and A. N. Pinto are with the Department of Electronics, Telecommunications and Informatics, University of Aveiro and Instituto de Telecomunicações, 3810-193, Aveiro, Portugal (e-mail: sofia.amado@ua.pt).

F. P. Guiomar, L. Bertignono, and A. Carena are with Dipartimento di Elettronica e Telecominicazioni, Politecnico di Torino, 10129 Torino, Italy.

A. Nespola is with Istituto Superiore Mario Boella, 10138 Torino, Italy.

its non-rectangular (cross QAM) constellation structure, it requires a more complex transmitter structure to implement a correlated I-Q modulation and does not allow Gray coding [26]. Alternatively, time- or frequency-hybrid superchannel solutions could also be considered. In [27], we proposed a 400G frequency-hybrid triple-carrier superchannel solution, composed of a central PM-64QAM and two edge PM-16QAM carriers. When compared to the PM-32QAM carriers superchannel, the proposed hybrid solution will make the superchannel more resilient to reconfigurable optical add-drop multiplexer based on wavelength selective switch (ROADM-WSS) filtering due to the use of PM-16QAM carriers at the edges of the superchannel (which can operate at a lower power and also presents higher filtering tolerance than PM-32QAM carriers) [28], [29], whilst avoiding the use of non-square QAM carriers.

Since in optical transmission systems based on hybrid solutions the different formats may have quite different performances, a new flexible forward error correction (FEC) technique has been proposed as a way to improve the overall system capacity. In [30] this approach was applied to a TDHMF system, based on hybrid PM-QPSK and PM-16QAM modulation, where each format operates with its own FEC code, providing an improvement of the system sensitivity compared to a single FEC approach. This technique was also applied to a superchannel system [31] and to a full WDM C+L-band transmission system [32], [33] aiming to counteract performance variations between different carriers and/or channels.

In [27], the optimum PR between carriers was analytically determined for the linear and nonlinear regimes of operation through the EGN model and verified by experimental and simulative (split-step based) results. The superchannel was evaluated considering only linear compensation of the transmission impairments. In this paper, we evaluate the performance after linear and nonlinear compensation, considering three distinct FEC coding schemes. Additionally, we also analyze the impact of different digital backpropagation (DBP) techniques targeting intra- or inter-carrier compensation. The proposed superchannel solution proved to be compatible with the 62.5 GHz grid slot, thus enabling a spectral efficiency of 6.4 b/s/Hz, while achieving a maximum transmission distance of 2500 km.

The paper is organized as follows. The laboratorial setup utilized for the transmission of the proposed 400G superchannel, together with the digital signal processing (DSP) subsystems required to demodulate each superchannel carrier are described in Section II. In Section III, the performance of each carrier is individually assessed in terms of maximum reach, for both linear and nonlinear compensation. Section IV is devoted to the optimization of the PR between superchannel carriers for each of the FEC schemes considered. Then, in Section V, different DBP-based nonlinear mitigation strategies are applied aiming to evaluate their impact on the optimum PR and system maximum reach. Finally, the main conclusions drawn from this work are summarized in Section VI.

II. Experimental Setup

Fig. 1 illustrates the experimental setup used for the transmission of a WDM system composed of nine 400G frequency-hybrid superchannels. Each superchannel is assigned to a grid slot of 62.5 GHz (net SE of 6.4 b/s/Hz) and is composed of three carriers separated by 20 GHz: two PM-16QAM edge carriers and a central PM-64QAM carrier, each operating at a symbol rate of 18 GBaud, see the inset of Fig. 1. The proposed superchannel carries a gross bit-rate of 504 Gb/s, enabling to allocate 26% of overhead (including 20% of soft-decision FEC (SD-FEC) and 6% protocol overheads) over the net 400 Gb/s bit-rate, so that the system can operate at a pre-FEC bit error rate (BER) of 2.4×10^{-2} [8].

The central superchannel carriers (superchannel under test) are generated by 3 external cavity lasers (ECL) (linewidth $<$ 100 kHz), while the remaining 24 carriers are generated by distributed feedback lasers (DFB). The central PM-64QAM optical carrier is modulated using a dual-polarization in-phase and quadrature modulator (DP-IQM), driven by a digital-to-analog converter (DAC) operating at 64 GSa/s and with an electrical bandwidth of 8 GHz. A second DAC is used to create two independent 16QAM signals, which are then polarization multiplexed by means of a polarization multiplexer (PM) emulator, yielding the two edge PM-16QAM carriers. The modulation signals are obtained from uncorrelated 2^{15}-1 pseudo-random bit-sequences (PRBSs), digitally shaped by a raised cosine filter with a roll-off factor of 0.05, and pre-emphasized to compensate for the bandwidth limitations of the transmitter components. After coupling the optical carriers, the PR between superchannel carriers, defined as $P_{64\mathrm{QAM}}/P_{16\mathrm{QAM}}$, is adjusted by a programmable optical filter placed at the optical coupler output, before an erbium doped fiber amplifier (EDFA). Note that, the PR between carriers is identically adjusted for all the 9 WDM superchannels.

The generated 9 WDM 400G superchannels are then launched into the optical recirculating loop, controlled by two acousto-optic modulators (AOM) and composed of 2×107.62 km spans of pure silica core fiber (PSCF) (each span consisting of 54.44 km of PSCF150 plus 53.18 km of PSCF110). Each fiber span is composed of concatenated spools of PSCF150 and PSCF110 fiber, whose weight average parameters are [34]: attenuation (α) is 0.16 dB/km; chromatic dispersion (CD) is 20.6 ps/nm/km; nonlinear coefficient (γ) is 0.7 $\mathrm{W^{-1}km^{-1}}$. Additionally, there are about 1.5 dB of extra losses per span due to the splices between PSCF transition patch-cords and fiber spools. A loop synchronous polarization scrambler (LSPS) is inserted to average out polarization dependent effects in the loop. After each fiber span, an EDFA, with 5.5 dB of noise figure, compensates for the total span loss of 18.75 dB. The loop also includes a gain-equalizer unit (Gain Eq) required to correct for residual gain unbalance and to preserve the PR between carriers.

After the recirculating loop, a standard coherent receiver detects each carrier of the central superchannel, tuning the local oscillator (LO) laser (ECL laser) and the optical filter to the desired carrier. A 25 GHz bandwidth tunable

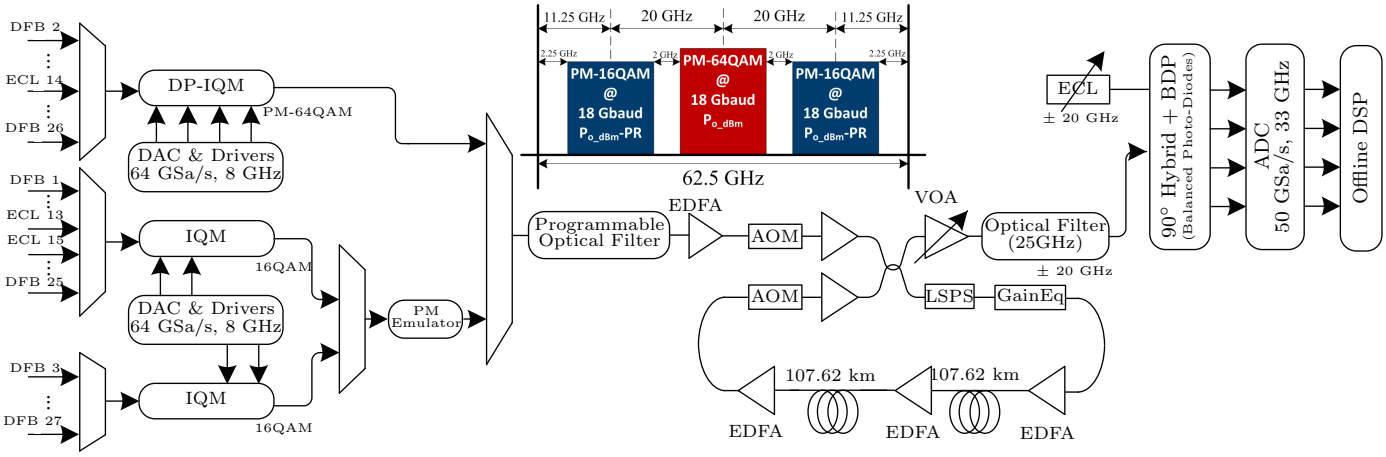

Fig. 1: Experimental setup for the nine 400G superchannel WDM transmission system. The inset shows the proposed frequency-hybrid superchannel composed of a central PM-64QAM carrier and two edge PM-16QAM carriers, each carrier operating at 18 GBaud.

optical filter is inserted at the receiver input, aiming to prevent excessive optical power from reaching the photo-detectors. The signal is then sampled by a 50 GSa/s real-time oscilloscope with an analog bandwidth of 33 GHz and offline DSP is independently applied to each carrier. The DSP starts with the compensation of the optical frontend impairments, low-pass filtering and downsampling to 2 samples per symbol (SpS). A static equalizer block is then applied to perform chromatic dispersion equalization (CDE) in frequency-domain, or alternatively intra-carrier nonlinear compensation based on a split-step Fourier DBP technique. After that, a 2x2 multi-input multi-output radius-directed equalizer (RDE) [35], [36] is independently applied to each superchannel carrier to compensate for the polarization-dependent effects and residual CD. For the PM-16QAM carriers, the RDE equalizer is initialized in a data-aided (DA) mode, with the correct radii of the 16QAM constellation being known a priori from a training sequence. After tap convergence is reached, the RDE equalizer is switched to a decision-directed (DD) mode [35], [36]. In turn, for the PM-64QAM carrier, the RDE equalizer is kept in DA mode at all times, in order to avoid possible tap divergence issues. Note that, when using SC-FEC, the PM-64QAM carrier can operate in a high BER regime, which may be more challenging for the equalizer convergence and stability. The use of fully DA equalization for the PM-64QAM carrier has therefore been a design choice to ensure more robust equalization, thereby avoiding any interference of possible DSP implementation issues on the performance analysis of the frequency-hybrid 400G SC, which is the main focus of this paper. Nevertheless, we do not expect this simplified DSP assumption to create significant performance changes, since it has been already shown in other works that blind DSP can be adequately designed for PM-64QAM with very small implementation penalty [36]. Then, frequency estimation is performed by a 4th power spectral method, while an initial coarse phase estimation based on the 4th-power Viterbi&Viterbi (V&V) algorithm is applied to the QPSK-like symbols in the PM-16QAM and PM-64QAM carriers. Although this V&V CPE stage is applied over the $2\times$ oversampled signal, phase estimation is actually performed over a downsampled version of the signal (1 sample/symbol). The extracted phase noise trace is then upsampled to 2 samples/symbol and removed from the signal, allowing for a subsequent fractionally-spaced FIR-based adaptive equalization stage. An additional inter-symbol interference (ISI) 4x4 adaptive equalizer is required after CPE for fine tuning the linear adaptive equalization, and to compensate for the residual IQ transmitter skew. This equalizer is based on a least mean square (LMS) algorithm, with a DA convergence stage followed by DD operation in steady-state for the PM-16QAM carriers and fully-DA operation for the PM-64QAM carrier, with the real and imaginary parts of each signal polarization being treated separately. At the end, the signal is downsampled to 1 SpS and a second fine-tuned CPE stage based on a maximum likelihood decision-directed (ML-DD) algorithm, using 31 taps, is applied [37]. Note that, the number of taps used by each algorithm is optimized for the two modulation formats. Finally, after signals decoding, the BER associated to each superchannel carrier is estimated.

The system was initially evaluated in a back-to-back (B2B) configuration, aiming to determine the implementation penalties associated to each superchannel carrier, which affect the theoretical predictions of the system performance. Considering the defined BER threshold of 2.4×10^{-2}, the experimental B2B penalties associated with the PM-16QAM and PM-64QAM carriers were determined to be 0.8 dB and 2.3 dB, respectively. Afterwards, the experimental setup was analyzed for different values of PR. For each PR, we varied the input mean power per superchannel between -8 dBm and 2 dBm, and the number of loop recirculations, ranging from 1 recirculation up to a maximum of 20 recirculations (about 4300 km).

Along this paper, unless otherwise mentioned, the plotted curves (dashed, dotted, solid lines) refer to the EGN model predictions, the open markers (△, ▽, ○, □) refer to the simulation results and the filled markers (▲, ▼, ●, ■) refer to the experimental results. The PM-16QAM experimental and simulation results shown are obtained from the mean BER of the two PM-16QAM edge carriers.

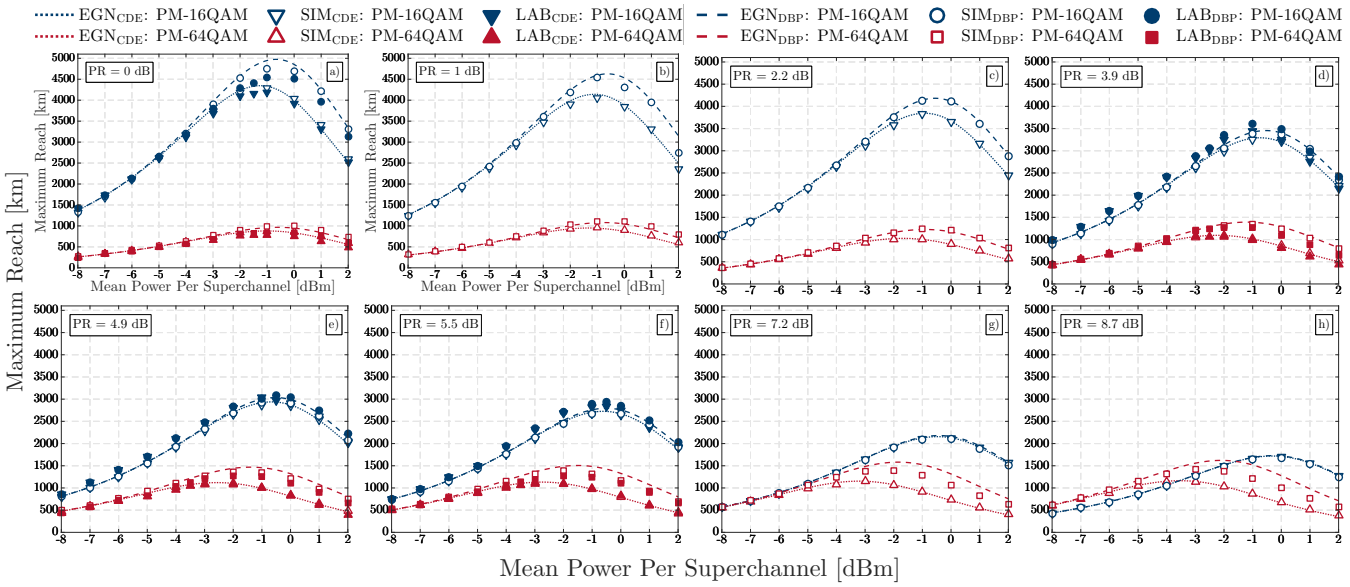

Fig. 2: Maximum reach as a function of the mean power per superchannel, considering different values of PR between carriers, for both CDE (dotted-curves, △, ▲, ▽, ▼ markers) and DBP (dashed-curves, □, ■, ○, ● markers) cases of each superchannel carrier (in the channel under test). Curves: EGN model predictions; Filled markers: experimental results; Open markers: simulative results. The dashed lines correspond to the average performance of the two PM-16QAM edge carriers, and the dotted lines to the PM-64QAM carrier performance.

III. Individual Performance Analysis of each Superchannel Carrier

In this section, we evaluate the performance of each superchannel carrier individually determining the maximum reach (MR) when a BER threshold of 2.4×10^{-2} is reached (assumption of a 20% SD-FEC). Analysis is conducted either considering regular chromatic dispersion equalization (label CDE) or nonlinear compensation through DBP (label DBP), where DBP is employed separately to each carrier. The system is initially analyzed from the theoretical point of view by taking advantage of the EGN model, which allow us to account for the different modulation formats assigned to each superchannel carrier, and then validated by experimental and simulative results. The experimental results are obtained using the setup presented in the previous section, while split-step-based simulations are carried out using the commercial optical system simulator OptSim™. For uniformity with the experimental scenario, B2B penalties are taken into account by noise loading over the received signal in the simulation, and by adjusting the target optical signal-to-noise ratio (OSNR) in the EGN model.

Fig. 2 presents the estimated MR of each carrier as a function of the mean power per superchannel and PR, for CDE (dotted-curves and △, ▲, ▽, ▼ markers) and DBP (dashed-curves and □, ■, ○, ● markers) cases. Both in experiment and simulation, DBP is applied using the back-propagation split-step Fourier (BP-SSF) method with 2 steps per span. For the EGN model, we first evaluate the NLI produced by the transmission of a single-carrier under analysis, that is being compensated by DBP, then in the post-processing it is removed from the total NLI affecting the carrier (when considering the transmission of all the 9 superchannels). The experimental and simulative MRs presented as a function of the mean power per superchannel are obtained from the interpolation of the BER results obtained after each recirculation, every 2 spans. As expected, the PM-64QAM carrier (red results) shows a shorter MR than PM-16QAM (blue results) for low PRs, not only due to the higher OSNR required for the PM-64QAM to deliver the mentioned BER threshold but also due to its higher sensitivity to nonlinear propagation effects (mainly because of the smaller guard band separating the PM-64QAM from its two PM-16QAM nearest neighbors). However, for high PRs, the carriers performances tend to be leveled out. It can be observed that the PR increase involves a compromise between the MR achieved by the PM-16QAM and PM-64QAM carriers, triggered by the inter-carrier NLI. Increasing PR cause a reduction of the MR achieved by the PM-16QAM carrier, due to the fact that we are reducing the power relatively to the PM-64QAM carrier, thereby the PM-16QAM will suffer from higher inter-carrier NLI produced by the adjacent high power PM-64QAM carriers. On the other hand, the MR achieved by the PM-64QAM increases due to the lower inter-carrier NLI generated by the adjacent reduced power PM-16QAM carriers.

When DBP is applied, there is a clear improvement of the superchannel carriers MR. However, as PR increases, the nonlinear compensation effect over the PM-16QAM carriers tends to become less pronounced, due to the fact that we are decreasing its power and consequently the nonlinearities caused by the carrier over itself, that are compensated for the DBP. On the other hand, the PM-64QAM carrier performance significantly improves not only due to the compensation of intra-carrier nonlinearity, but also due to the lower nonlinear effects caused by the adjacent carriers. Indeed, for PR of 2.2 dB, a MR increase of ∼20% and ∼9% is obtained for the PM-64QAM (∼1200 km against ∼1000 km) and PM-16QAM

carriers (∼4150 km against ∼3800 km), respectively. In turn, for higher PRs, such as 8.7 dB, a MR gain of ∼40% is obtained for the PM-64QAM carrier (∼1650 km against ∼1150 km), while it becomes negligible for the PM-16QAM carriers.

In general, there is an excellent agreement of the experimental results with the EGN model and simulation analysis, see Fig. 2. Only for few cases based on DBP there is a small misalignment between results, but differences are always limited to less than 15%, which may be due to the presence of stronger nonlinear signal-to-noise interactions in the optical link and also due to the possible correlations between the various carriers in the laboratorial experiment (resulting from the even-odd modulation) [38], [39]. This comprehensive study on the individual performance of superchannel carriers allowed us to make sure that both EGN model and simulation analysis are fully aligned with the experiment proving that an accurate parameter identification has been successfully conducted. Under these conditions, in the next sections of the paper we can proceed to the application of different FEC and compensation strategies having reliable results from experiment, simulation and model. Moreover, based on such confidence, in Section V we will use the EGN model to extend our analysis further than the set of experimental data to demonstrate some advanced approach for DBP.

IV. Joint Power-Ratio and FEC Optimization

In this section, we assess the overall superchannel performance aiming to determine the optimum PR between superchannel carriers. We consider the following three FEC paradigms:

- **Superchannel FEC (SC-FEC)**, consisting of a single FEC code applied to the single 400G data stream carried by the three carriers composing the superchannel. Fig. 3a depicts the block diagram of SC-FEC implementation. A single FEC encoder is applied to the entire data stream of a superchannel, which is then sent to an interleaver block that decorrelates the data stream over time and across the superchannel carriers. After that, a serial to parallel conversion (S/P) block is applied to divide the data stream into the carriers data streams. Afterwards, each carrier is independently modulated and combined in a superchannel for transmission. At the receiver, after independent demodulation of the each superchannel carrier, the data streams are combined again by a parallel to serial conversion (P/S) block and send to the de-interleaver block. A single FEC decoder block is then applied to the entire superchannel data stream, aiming to retrieve the transmitted bits. In this work, the superchannel FEC overhead (FEC-OH) is defined as 20 %. Since FEC coding and decoding is interleaved among all superchannel carriers, the system performance can be assessed through the pre-FEC weighted average BER given by:

$$\mathrm{BER_{SC}} = \frac{\sum_n \log_2(M_n)\mathrm{BER_n}}{\sum_n \log_2(M_n)}, \quad (1)$$

where $\mathrm{BER_{SC}}$ is the average BER of the entire superchannel, $\mathrm{BER_n}$ is the BER measured on the n-th superchannel carrier and M_n is the constellation cardinality of the n-th superchannel carrier.

- **Independent carrier FEC (IC-FEC)**, consisting of N independent FEC codes, one for each superchannel carrier, with a fixed and common OH. In this case, independent FEC encoder and decoder blocks are applied to each carrier of the superchannel, as can be seen from Fig. 3b. In this work, all carriers operate with the same FEC-OH of 20%. Since all superchannel carriers are coded and decoded independently, the overall superchannel performance is set by the worst performing carrier and thus can be assessed by the highest individual pre-FEC BER:

$$\mathrm{BER_{SC}} = \max(\mathrm{BER_n}). \quad (2)$$

Therefore only the worst performing carrier is operating at the FEC threshold, while the remaining carriers are practically working error free with some margin with respect to the FEC threshold.

- **Independent carrier flexible FEC (Flex-FEC)**, in which, similarly to the IC-FEC case, an independent FEC code is assigned to each carrier, but the allocated OHs can be optimized on a per-carrier basis. In order to maintain a net bit-rate of 400 Gb/s and thereby allow for a fair comparison with the SC-FEC and IC-FEC approaches, in this work we constrain the total superchannel Flex-FEC overhead $\mathrm{OH_{SC}}$ (weighted average of all FEC-OHs per carrier) to 20%. Considering that the two PM-16QAM edge carriers should exhibit a similar performance, we constrain them to have same OH. For a given OH in the PM-64QAM carrier, $\mathrm{OH_{64QAM}}$, the correspondent OH in the PM-16QAM carriers $\mathrm{OH_{16QAM}}$ is given by:

$$\mathrm{OH_{16QAM}} = \frac{(\sum_n \log_2(M_n))\mathrm{OH_{SC}}}{\log_2(M_{16QAM}) \times 2} - \frac{\log_2(M_{64QAM})\mathrm{OH_{64QAM}}}{\log_2(M_{16QAM}) \times 2}, \quad (3)$$

where the 2 factor is accounting for the two PM-16QAM edge carriers. Then, similarly to the IC-FEC case, the superchannel performance with Flex-FEC coding can be assessed from the maximum pre-FEC BER among all carriers, equation (2). However, in this case, the limit pre-FEC BER must be adjusted according to the OH required by each FEC, details are introduced later in this section.

For the application of the Flex-FEC strategy, Fig. 4 shows the pre-FEC BER as a function of FEC-OHs. We took advantage of the values presented in [8], Table I, to determine the new pre-FEC BER associated to each OH. Considering the constraint of an overall $\mathrm{OH_{SC}}$ = 20%, we present the considered values of PM-64QAM OH ($\mathrm{OH_{64QAM}}$) and the correspondent PM-16QAM OH ($\mathrm{OH_{16QAM}}$).

Taking into account the determined new BER thresholds associated to each modulation format, the B2B penalties were re-calculated from experimental B2B characterization and the EGN model was re-evaluated for PRs ranging between 0 and 10 dB for all the OHs presented in Fig. 4, aiming to find the set of OHs ($\mathrm{OH_{64QAM}}$, $\mathrm{OH_{16QAM}}$) providing the best performance

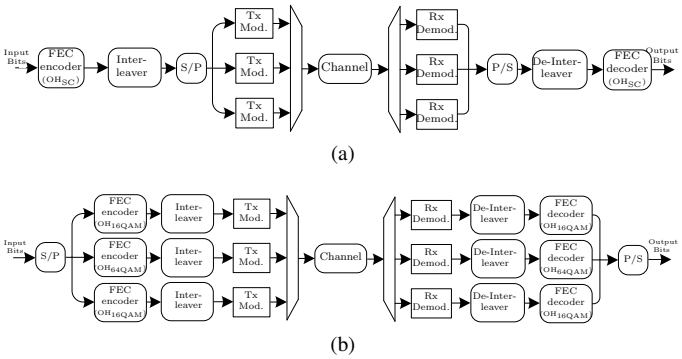

Fig. 3: Block diagram for the implementation of the considered FEC paradigms: a) SC-FEC (OH_{SC} = 20%) and b) IC-FEC (OH_{16QAM} = OH_{64QAM} = OH_{SC} = 20%) or Flex-FEC ($OH_{16QAM} \neq OH_{64QAM}$ but OH_{SC} = 20%).

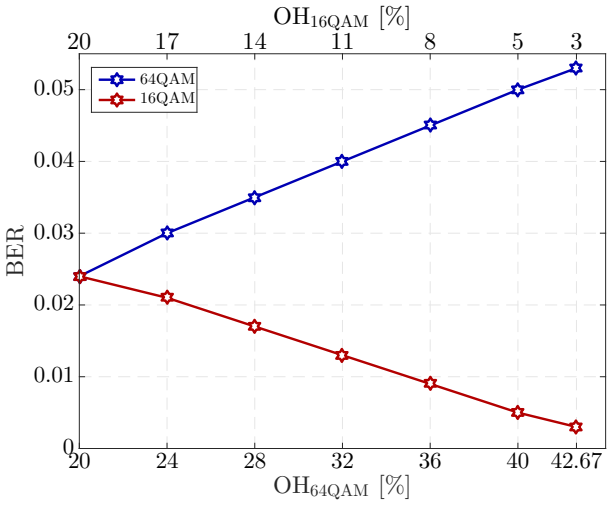

Fig. 4: Pre-FEC BER as a function of the OH_{64QAM} (bottom X axis) and respective OH_{16QAM} (top X axis), for a pos-FEC BER of 1×10^{-15}. The markers correspond to the set of OHs (OH_{64QAM}, OH_{16QAM}) considered in this work. Note that, the OH_{64QAM}=20% (OH_{16QAM}=20%) point corresponds to the IC-FEC strategy.

for the Flex-FEC strategy. Fig. 5, presents the MR as a function of the PR between carriers, for the set of FEC-OHs considered in Fig. 4, when CDE is applied. In our hybrid scenario, we achieve the best performance when increasing the OH_{64QAM}, while reducing the OH_{16QAM}, in order to maintain a total OH_{SC} of 20%, corresponding to 400 Gb/s of net bit-rate. Increasing OH_{64QAM} allow us to operate at a higher pre-FEC BER, thereby extending the MR of this carrier. From Fig. 5 we can determine the MR and correspondent optimum PR for each set of FEC-OHs being considered (for CDE only). The same EGN-based analysis has also been performed considering DBP. The MR obtained at the optimum PR as a function of the FEC-OHs is shown in Fig. 6, for both CDE and DBP cases. As expected, the increase of OH_{64QAM} enables a gradual increase of MR up to ∼1940 km and ∼2300 km (corresponding to an improvement of ∼70% and ∼50% with respect to the IC-FEC strategy, as we will see later on), jointly with a reduction of 6.5 dB and 5 dB in the optimum PR, respectively for the CDE and DBP compensation. The optimum set of FEC-OHs is found for OH_{64QAM} = 40%/OH_{16QAM} = 5% for CDE and OH_{64QAM} = 36%/OH_{16QAM} = 8% for DBP. After these points, system performance starts deteriorating again, since it becomes limited by the reduced reach of the PM-16QAM carrier, due to its very low OH_{16QAM}.

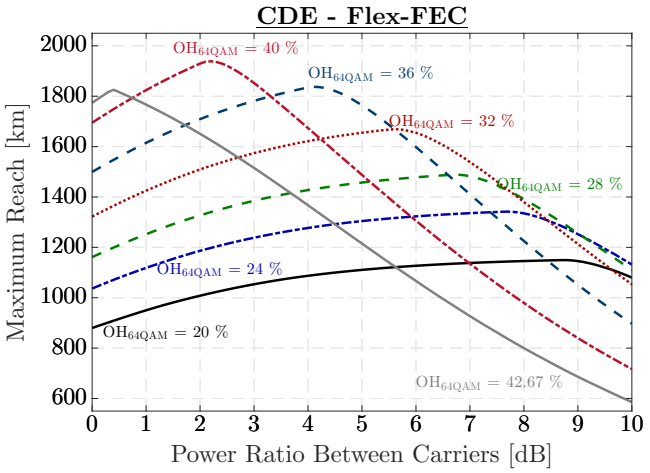

Fig. 5: Maximum reach as a function of the power-ratio for different sets of FEC-OHs, when CDE is applied.

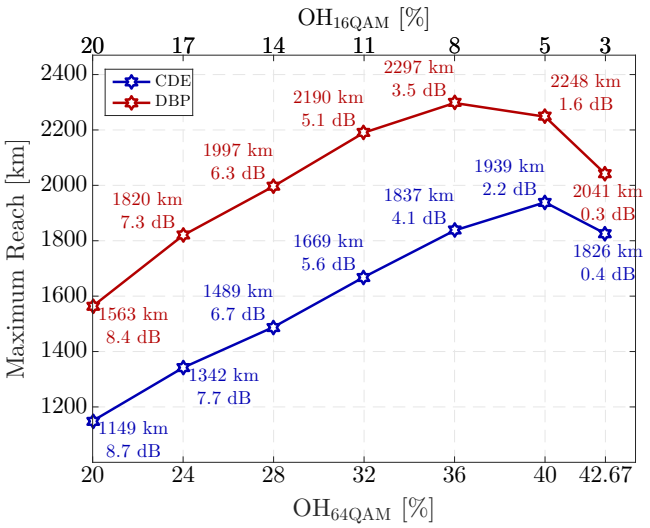

Fig. 6: Maximum reach as a function of the OH_{64QAM} (bottom X axis) and OH_{16QAM} (top X axis), for both CDE (blue curve) and DBP (red curve) cases. Note that, for each set of FEC-OHs the correspondent maximum reach and optimum power ratio are specified.

Now, if we consider the theory for AWGN channels devised in [21], the optimum performance for the IC-FEC and SC-FEC strategies would require PRs of 5.7 dB and 3.6 dB, respectively, for a target BER of 2.4×10^{-2}. However, these results do not take into account any modulation format dependent implementation penalties. In this work, due to the different B2B penalties associated with PM-16QAM (0.8 dB) and PM-64QAM (2.3 dB), the required nominal PRs are increased to 7.2 dB and 4.4 dB for the IC-FEC and SC-FEC strategies, respectively. In fact, in Fig. 2g (PR=7.2 dB) it can be observed that both modulation formats are performing similarly in the linear propagation regime (the two curves overlap, thereby operating at same BER). However, when the

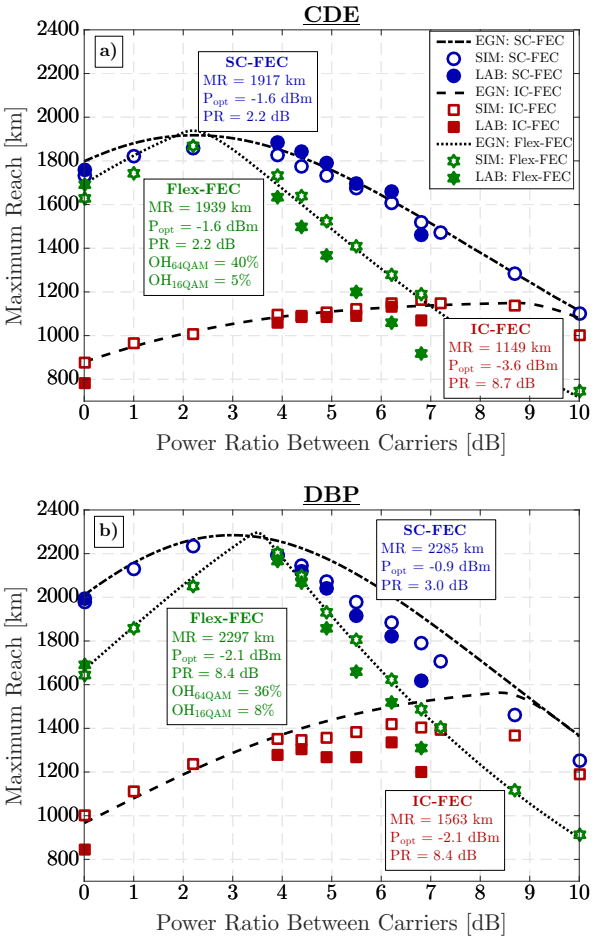

Fig. 7: System performance in terms of maximum reach as a function of PR for all FEC strategies, when applying a) CDE and b) DBP on each superchannel carrier. Dashed-dotted, dashed and dotted lines correspond to the EGN model predictions for the SC-FEC, IC-FEC and Flex-FEC operation strategies, respectively. Filled and open markers correspond to experimental and simulative results, respectively.

system enter in a nonlinear regime due to the different NLI generation, because of PR, the optimal condition derived in B2B is not anymore valid, as it has been simulatively shown in [40] for a system with similar frequency-hybrid properties. After running the EGN model for PRs ranging between 0 and 10 dB, we observed that the MR for the IC-FEC and SC-FEC strategies is in fact achieved for PRs of 8.7 dB and 2.2 dB, respectively, see Fig. 7a. In the IC-FEC strategy, the global MR is set by the worse performing carrier at the optimum superchannel launched power, therefore originating two different regions of operation: i) at low PR, the system MR and optimum power are set by the worse performing modulation format (the PM-64QAM is limiting the achievable MR, since in this case the PM-16QAM always outperforms the PM-64QAM, see Fig. 2); ii) at high PR, the system MR and optimum power are set by the crossing point between the individual carrier MR curves of each modulation format, which are consequently operating at the same BER. The best system performance is achieved on the transition between these two regimes of operation, occurring in the considered scenario for a PR of 8.7 dB (as can be confirmed from Fig. 7a). After this point, the maximum system performance starts to be limited by the PM-16QAM carrier still operating in the linear regime, owing to its very low power, while the PM-64QAM is already operating in nonlinear regime. In turn, for the SC-FEC strategy, the system MR and optimum power require a continuous balanced compromise between the two modulation formats, since these are determined from the weighted average BER of the superchannel. In the considered scenario, since the PM-16QAM carriers simultaneously enable higher reach and also transport more data (2×4 bits per symbol, against 6 bits per symbol of the PM-64QAM carrier), the maximum performance of the system is achieved for a relatively low PR of 2.2 dB, which provides the best compromise between the two formats in terms of average superchannel BER.

All previous conclusions are summarized in Fig. 7, where we show the MR as a function of PR for all three FEC paradigms. Note that, in the Flex-FEC case, we only present the curve corresponding to the best FEC-OH pair, $\mathrm{OH_{64QAM}}$/$\mathrm{OH_{16QAM}}$. In the considered scenario, the PR optimization allows for a MR extension of <10%, ∼30% and ∼15% (CDE only) for the SC-FEC, IC-FEC and Flex-FEC strategies, respectively, see Fig. 7a. From the FEC paradigms point of view, the theoretical, simulation and experimental results show that the SC-FEC strategy always outperform IC-FEC strategy in terms of MR. For PR=0 dB, the SC-FEC strategy enables to double the reach provided by IC-FEC. Instead, considering the optimum PR operation points for each FEC strategy (2.2 dB for SC-FEC and 8.7 dB for IC-FEC), MR gain provided by SC-FEC is ∼70%. On the other hand, we can note that by adjusting the FEC-OHs of each modulation format (Flex-FEC strategy), we can achieve approximately the same MR (∼1% gain using Flex-FEC) of the SC-FEC under the same conditions of operation (PR and optimum launched power). We also demonstrate that applying DBP the MR achieved with the SC-FEC/Flex-FEC and IC-FEC strategies can be further improved by ∼20% and ∼35%, respectively, see Fig. 7b. Besides, as consequence of DBP, the optimum PR for the SC-FEC and Flex-FEC strategy increases to 3 dB and 3.5 dB, due to the higher launched power coming along with the application of DBP. It is also worth noting that the optimization of PR becomes significantly more important when applying DBP. In this case, the MR extension provided by optimized PR is of ∼15% (from ∼2000 km to ∼2300 km), ∼60% (from ∼960 km to ∼1560 km) and ∼40% (from ∼1650 km to ∼2300 km) for the SC-FEC, IC-FEC and Flex-FEC strategies, respectively.

Another key system parameter is the optimum launched power per superchannel (P_{opt}), i.e. the mean launched power per superchannel corresponding to the MR. We collected the P_{opt} values for all FEC implementation strategies, for both CDE and DBP cases, plotting it as a function of the PR in Fig. 8. It can be observed that the lower PR and higher MR provided by the SC-FEC and Flex-FEC strategies comes at the expense of a 2 dB higher optimum launched mean power (P_{opt}=-1.6 dBm against P_{opt}=-3.6 dBm for the IC-FEC strategy, considering CDE). The application of DBP will also produce an impact on the optimum launched power,

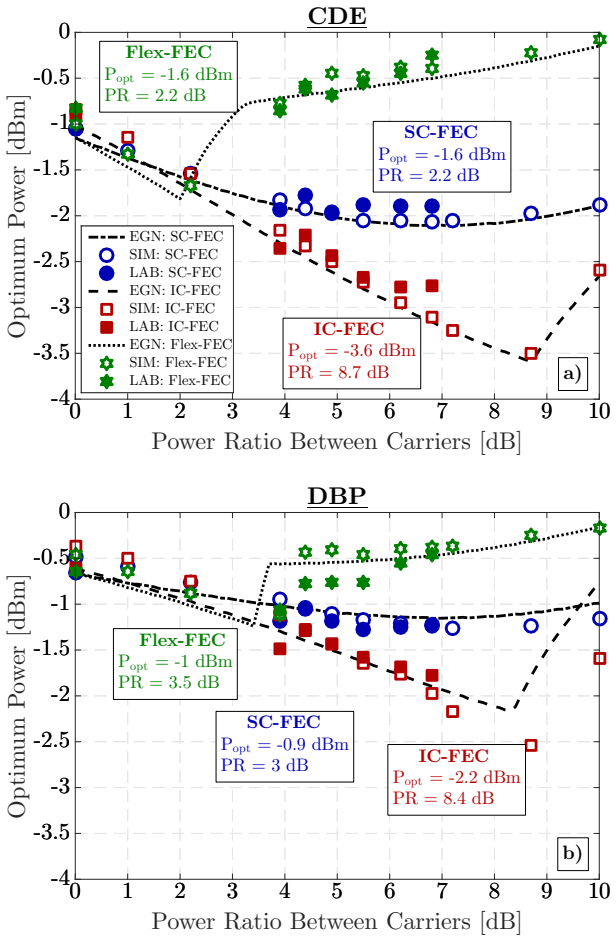

Fig. 8: Optimum mean power per superchannel as a function of PR for all FEC strategies, when applying a) CDE and b) DBP on each superchannel carrier. Dashed-dotted, dashed and dotted lines correspond to the EGN model predictions for the SC-FEC, IC-FEC and Flex-FEC operation strategies, respectively. Filled and open markers correspond to the simulation and experimental results, respectively.

besides its impact on the optimum PR and MR. Indeed, we observe that after DBP P_{opt}increases to -0.9 dBm (PR=3 dB), -1 dBm (PR=3.5 dB) and P_{opt}=-2.2 dBm (PR=8.4 dB) for the SC-FEC, Flex-FEC and IC-FEC strategies, respectively. This corresponds to a P_{opt} nonlinear tolerance improvement of 0.7 dB, 0.6 dB and 1.4 dB , respectively. The previous 2 dB difference in the optimum powers between SC-FEC/Flex-FEC and IC-FEC operation strategies (see Fig. 8a) is now reduced to about 1 dB (see Fig. 8b). The abrupt change of behavior of the Flex-FEC P_{opt} curve is due to the transition between different regimes of operation: initially P_{opt} is set by the PM-64QAM carrier (in the regime where its performance is worse than PM-16QAM), while then, there is a PR for which the two modulation format curves cross and P_{opt} becomes defined by the intersection between the two curves (one in the nonlinear regime and the other in the linear regime). By increasing even more the PR, there will be a point where P_{opt} starts to be given by the PM-16QAM carrier, since its maximum performance becomes worse than that of PM-64QAM for all average launched power per superchannel. Note that this transition occurs more steeply in the DBP case.

From the previous analysis, we can conclude that the IC-FEC strategy can be considered as a lower bound, being limited by the highest BER among all superchannel carriers. On the other hand, the SC-FEC strategy tends to present a better performance at the expense of requiring the application of a single FEC to the entire superchannel, aiming to interleave the bit errors of the worst performing carrier with the bit errors of the remaining carriers. Alternatively, the application of an optimized FEC-OH to each modulation format allow us to nearly achieve the same performance of the SC-FEC (under same operation conditions). However, the performance of the Flex-FEC strategy around its optimum PR value was found to vary more abruptly, both in terms of MR and in terms of P_{opt}.

V. Advanced Strategies for Nonlinear Compensation

In this section, we use the EGN model to extend the previous analysis considering different methods for the application of nonlinear compensation to the superchannel under test. Up to this point, we have been considering DBP applied to all three carriers individually, we now consider other three cases:

1) DBP is applied only to the two PM-16QAM edge carriers individually (DBP_{16QAM});
2) DBP is applied only to the center PM-64QAM carrier (DBP_{64QAM});
3) DBP is applied jointly to all three carriers forming the superchannel (DBP_{WB}, WB accounting for wideband).

Fig. 9 shows the EGN model predictions for CDE, DBP, DBP_{16QAM}, DBP_{64QAM} and DBP_{BW}, for all three FEC strategies. From Fig. 9a it can be seen that there is no significant enhancement of the system MR (<5%) when DBP is applied to all carriers (MR = 2285 km) compared to the case where DBP is applied only to PM-64QAM (MR = 2242 km).Thereby, the application of DBP only over the PM-64QAM carrier proves to be a convenient design option for the analyzed scenario, enabling a substantial complexity reduction. Alternatively, if DBP is applied jointly to the whole superchannel an additional ∼10% MR extension is achieved, which corresponds to an improvement of ∼30% over CDE. However, this case requires a wideband (WB) receiver and the joint detection of all three superchannel carriers, such that full field DBP can be applied. Considering that we employ 62.5 GHz frequency grid, today state-of-the art receivers allow a practical implementation of such approach, but due to limitations in our equipment we could not test it experimentally. Alternatively, we could also detect each carrier independently, through phase and time locked co-operating receivers, and then apply a coupled equations DBP, at the cost of additional implementation complexity [41]. These techniques enable to ideally remove for all deterministic fiber impairments, namely self phase modulation (intra-carrier nonlinearities), cross phase modulation and four wave mixing (inter-carrier nonlinearities).

Regarding the IC-FEC strategy, Fig. 9b shows that the DBP_{16QAM} does not bring any improvement over CDE, neither

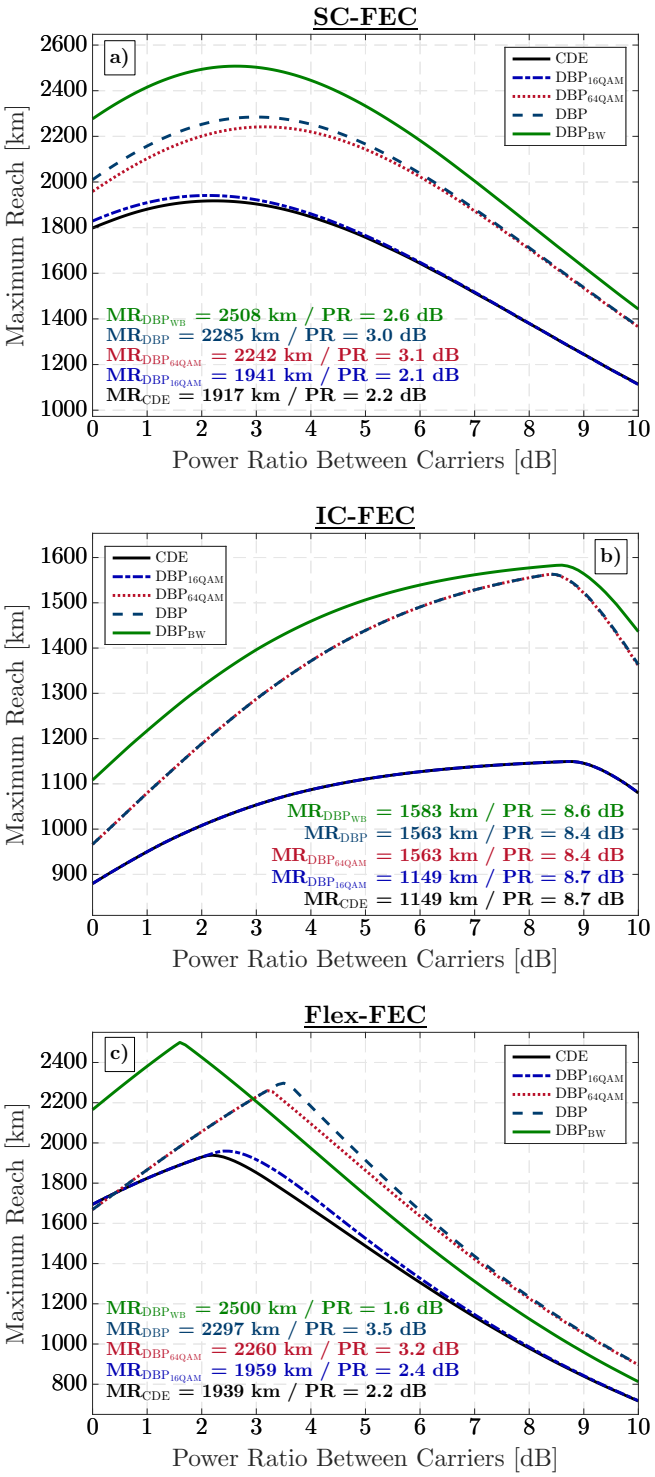

Fig. 9: Theoretical performance comparison, in terms of MR, for different DBP application strategies and for all three FEC paradigms: a) SC-FEC; b) IC-FEC and c) Flex-FEC. Black solid lines correspond to the CDE case; Dark blue dashed lines correspond to the DBP of all three superchannel carriers (DBP); Blue dashed-dotted lines correspond to the DBP of the edges PM-16QAM carriers (DBP_{16QAM}); Red dotted lines correspond to the DBP of the central PM-64QAM carrier (DBP_{64QAM}); Green solid lines correspond to the jointly DBP on all superchannel carriers.

over DBP_{64QAM}, since the system performance is being limited by the PM-64QAM (up to the crossing point between individual carrier MR curves). After such high PRs (>8 dB) NLI is mainly generated by the PM-64QAM carrier, as proved in the previous sections. In contrast with the previous case, DBP_{WB} with IC-FEC brings an improvement of only 1% on the achievable system MR (at the optimum PR).

Finally, in the case of Flex-FEC strategy, the gains provided by the application of each DBP strategy over CDE are identical to those obtained with SC-FEC ($\sim$ 20% using DBP and DBP_{64QAM} and $\sim$ 30% using DBP_{WB}), see Fig. 9c. Moreover, the application of DBP_{16QAM} is again insignificant over the DBP_{64QAM} and CDE. Comparing the results of Fig. 9a and 9c, we verified that the MRs obtained with the Flex-FEC (at the optimum PRs) are similar to those obtained with the SC-FEC (within 1% difference). However, in contrast with the SC-FEC case, for all DBP strategies, there is a steep performance degradation when we slightly change the PR.

VI. Conclusions

We have experimentally demonstrated the WDM performance optimization and transmission of nine 400G frequency-hybrid superchannels, composed of two edge PM-16QAM carriers and a central PM-64QAM carrier, designed to occupy a 62.5 GHz grid slot with a spectral efficiency of 6.4 b/s/Hz. The experimental results were complemented by split-step based OptSim™ simulations and analytical EGN model predictions.

We analyzed, for the first time to our knowledge, the critical issue of power-ratio optimization adjustment between the superchannel carriers and its impact on nonlinear propagation performance. The system has been evaluated in terms of maximum transmission distance and optimum average power per superchannel under three different FEC paradigms. The SC-FEC scheme, which is based on the average superchannel BER, was found to be the more robust approach for frequency-hybrid superchannels, as it shows a smoother dependence on power-ratio between carriers, thus tolerating larger uncertainty on the system optimization. In addition, SC-FEC does not require individual optimization of FEC overheads per carrier, thereby simplifying the implementation. In other words, the residual performance gain that can be achieved by Flex-FEC encoding requires a very precise optimization of several system parameters such as launched power, power-ratio and FEC overhead, that might not be feasible in a real scenario. As opposed to it, SC-FEC enables a simpler and more error-tolerant design of frequency-hybrid transmission systems.

We have also investigated the performance gain that can be provided by the application of different DBP techniques in the considered frequency-hybrid superchannel system, and its implications on the optimum power-ratio and launched power. We note that the unequal transmitted power per carriers sets unique new challenges and opportunities for the implementation of DBP in frequency-hybrid systems. Applying self-carrier interference DBP compensation to the PM-64QAM carrier only, we demonstrated a maximum transmission distance of $\sim$2300 km and $\sim$1600 km for the SC-FEC/Flex-FEC and IC-FEC strategies, respectively. Moreover,

we have also demonstrated that the nonlinear compensation of all carriers of a frequency-hybrid superchannel might not be worthwhile. Indeed, most of the benefit provided by DBP was achieved by the standalone compensation of the central PM-64QAM carrier (>95%), thereby enabling for a substantial reduction of DBP computational effort. Finally, an extended analytical study revealed that jointly compensating nonlinear impairments applying DBP to the overall superchannel signal received through a wideband receiver can potentially bring an additional improvement of about 10% over independent application of DBP for the SC-FEC/Flex-FEC strategy, while this gain becomes negligible for the IC-FEC strategy.

REFERENCES

[1] Infinera whitepaper, "Super-Channels DWDM Transmission Beyond 100Gb/s: Will Bandwidth Growth Ever Stop? No.," *http://www.infinera.com/pdfs/whitepapers/SuperChannel_WhitePaper.pdf*

[2] X. Zhou and L. E. Nelson, "400G WDM Transmission on the 50 GHz Grid for Future Optical Networks," *J. Lightw. Technol.*, vol. 30, no. 24, pp. 3779–3792, 2012.

[3] X. Zhou, L. E. Nelson, P. Magill, R. Isaac, B. Zhu, D. W. Peckham, P. Borel, and K. Carlson, "PDM-Nyquist-32QAM for 450-Gb/s perchannel WDM transmission on the 50 GHz ITU-T grid," *J. Lightw. Technol.*, vol. 30, no.4, pp. 553–559, 2012.

[4] G. Bosco, V. Curri, A. Carena, P. Poggiolini, and F. Forghieri, "On the Performance of Nyquist-WDM Terabit Superchannels Based on PM-BPSK, PM-QPSK, PM-8QAM or PM-16QAM Subcarriers," *J. Lightwave Technol.*, vol. 29, no. 1, pp. 53–61, 2011.

[5] T. Zeng, "Superchannel transmission system based on multi-channel equalization," *Opt. Express*, vol. 21, no. 12, pp. 14799–14807, 2013.

[6] C. Liu, J. Pan, T. Detwiler, A. Stark, Y. Hsueh, G. Chang, and S. E. Ralph, "Joint digital signal processing for superchannel coherent optical communication systems," *Opt. Express*, vol. 21, no. 7, pp. 8342–8356, 2013.

[7] D. Rafique, T. Rahman, A. Napoli, M. Kuschnerov, G. Lehmann, and B. Spinnler, "Flex-grid optical networks: spectrum allocation and nonlinear dynamics of super-channels," *Opt. Express*, vol. 21, no. 26, pp. 32184–32191, 2013.

[8] D. Rafique, T. Rahman, A. Napoli, S. Calabrò and B. Spinnler, "Technology Options for 400 Gb/s PM-16QAM Flex-Grid Network Upgrades," *Photonics Technology Letters*, vol. 26, no. 8, pp. 773–776, 2014.

[9] J.-X. Cai, H. G. Batshon, H. Zhang, M. Mazurczyk, O. Sinkin, D. G. Foursa, A. Pilipetskii, G. Mohs, and Neal S. Bergano, "30.4 Tb/s transmission over transpacific distance using 200 Gb/s and dual wavelength 400 Gb/s 16QAM at 6.0 b/s/Hz spectral efficiency," *Opt. Express*, vol. 22, no. 8, pp. 9116–9122, 2014.

[10] R. Maher, T. Xu, L. Galdino, M. Sato, A. Alvarado, K. Shi, S. J. Savory, B. C. Thomsen, R. I. Killey, and P. Bayvel, " Spectrally Shaped DP-16QAM Super-Channel Transmission with Multi-Channel Digital Back-Propagation," *Scientific Reports*, vol. 5, no. 8214, pp. 1–8, 2015.

[11] Z. Jia, H. C. Chien, J. Zhang, Y. Cai and J. Yu, "Performance Comparison of Dual-Carrier 400G With 8/16/32-QAM Modulation Formats," *IEEE Photonics Technology Letters*, vol. 27, no. 13, pp. 1414–1417, 2015.

[12] T. Rahman, D. Rafique, A. Napoli, E. de Man, B. Spinnler, M. Bohn, C. M. Okonkwo, A. M. J. Koonen, and H. de Waardt, "Ultralong Haul 1.28-Tb/s PM-16QAM WDM Transmission Employing Hybrid Amplification," *J. Lightwave Technol.*, vol. 33, no. 9, pp. 1794–1804, 2015.

[13] A. Napoli et al., "Next generation elastic optical networks: The vision of the European research project IDEALIST," *IEEE Communications Magazine*, vol. 53, no. 2, pp. 152–162, 2015.

[14] Q. Zhuge, M. Morsy-Osman, X. Xu, M. Chagnon, M. Qiu, and D. V. Plant, "Spectral Efficiency-Adaptive Optical Transmission Using Time Domain Hybrid QAM for Agile Optical Networks," *J. Lightw. Technol.*, vol. 31, no. 15, pp. 2621–2628, 2013.

[15] X. Zhou, L. E. Nelson, P. Magill, R. Isaac, B. Zhu, D. W. Peckham, P. Borel, and K. Carlson, "1200 km transmission of 50 GHz spaced, 5x504-Gb/s PDM-32-64 hybrid QAM using electrical and optical spectral shaping," presented at *Opt. Fiber Commun. Conf./Nat. Fiber Opt. Eng. Conf.*, Los Angeles, CA, USA, Mar. 4-8, 2012, Paper OM2A.2.

[16] X. Zhou, L. E. Nelson, P. Magill, R. Isaac, B. Zhu, D. W. Peckham, P. Borel, and K. Carlson, "High spectral efficiency 400 Gb/s transmission using PDM time-domain hybrid 32-64 QAM and training-assisted carrier recovery," *J. Lightw. Technol.*, vol. 31, no. 7, pp. 999–1005, 2013.

[17] F. P. Guiomar, R. Li, C. R. S. Fludger, A. Carena, and V. Curri, "Hybrid modulation formats enabling elastic fixed-grid optical networks," *J. Opt. Commun. Netw.*, vol. 8, no. 7, pp. A92–A100, 2016.

[18] F. Buchali, et al. "Rate adaptation and reach increase by probabilistically shaped 64-QAM: An experimental demonstration," *Journal of Lightwave Technology*, vol.34, no.7, pp. 1599–1609, 2016.

[19] J. Cho, et al. "Trans-Atlantic Field Trial Using Probabilistically Shaped 64-QAM at High Spectral Efficiencies and Single-Carrier Real-Time 250-Gb/s 16-QAM," presented at *Opt. Fiber Commun. Conf.*, Los Angeles, CA, USA, Mar. 19-23, 2017, Paper Th5B.3.

[20] K. Roberts, Q. Zhuge, I. Monga, S. Gareau and C. Laperle, "Beyond 100 Gb/s: capacity, flexibility, and network optimization," *J. Opt. Commun. Netw.*, vol. 9, no. 4, pp. C12–C23, April 2017.

[21] V. Curri, A. Carena, P. Poggiolini, R. Cigliutti, F. Forghieri, C. Fludger, and T. Kupfer, "Time-division hybrid modulation formats: Tx operation strategies and countermeasures to nonlinear propagation," presented at *Opt. Fiber Commun. Conf.*, San Francisco, CA, USA, Mar. 9-14, 2014, Paper Tu3A.2.

[22] A. Carena, G. Bosco, V. Curri, Y. Jiang, P. Poggiolini, and F. Forghieri, "EGN model of non-linear fiber propagation," *Opt. Express*, vol. 22, no. 13, pp. 16335–16362, 2014.

[23] F. P. Guiomar, S. B. Amado, R. M. Ferreira, J. D. Reis, S. M. Rossi, A. Chiuchiarelli, J. R. F. Oliveira, A. L. Teixeira, and A. N. Pinto, "Multi-Carrier Digital Backpropagation for 400G Optical Superchannels," *J. Lightw. Technol.*, vol. 34, no. 8, pp. 1896–1907, 2016.

[24] S. B. Amado, F. P. Guiomar, N. J. Muga, R. M. Ferreira, J. D. Reis, S. M. Rossi, A. Chiuchiarelli, J. R. F. Oliveira, A. L. Teixeira, and A. N. Pinto, "Low Complexity Advanced DBP Algorithms for Ultra-Long-Haul 400G Transmission Systems," *J. Lightw. Technol.*, vol. 34, no. 8, pp. 1793–1799, 2016.

[25] Y. Loussouarn, E. Pincemin, M. Song, S. Gauthier, Y. Chen, and Z. Shengqian, "400 Gbps Real-Time Coherent Nyquist-WDM DP-16QAM Transmission over Legacy G.652 or G.655 Fibre Infrastructure with 2 dB Margins," presented at *Opt. Fib. Commun. Conf.*, Los Angeles, CA, USA, Mar. 22-26, 2015, Paper W3E.3.

[26] E. Agrell, J. Lassing, E.G. Strom, T. Ottosson, "Gray coding for multilevel constellations in Gaussian noise," *IEEE Trans. Inf. Theory*, vol. 53, no. 1, pp.224–235, 2007.

[27] S. B. Amado, F. P. Guiomar, N. J. Muga, A. Nespola, L. Bertignono, A. Carena, and A. N. Pinto, "400G Frequency-Hybrid Superchannel for the 62.5 GHz Slot," presented at *Opt. Fiber Commun. Conf.*, Los Angeles, CA, USA, Mar. 19-23, 2017, Paper Th4D.4.

[28] T. Rahman, D. Rafique, B. Spinnler, A. Napoli, M. Bohn, T. Koonen, C. M. Okonkwo, and H. de Waardt, "Digital Subcarrier Multiplexed Hybrid QAM for Data-rate Flexibility and ROADM Filtering Tolerance," presented at *Opt. Fib. Commun. Conf.*, Anaheim, CA, 2016, Paper Tu3K.5.

[29] T. Rahman, A. Napoli, D. Rafique, B. Spinnler, M. Kuschnerov, I. Lobato, B. Clouet, M. Bohn, C. M. Okonkwo, and H. de Waardt "On the Mitigation of Optical Filtering Penalties Originating From ROADM Cascade," *Photonics Technology Letters*, vol. 26, no. 2, pp. 154–157, 2014.

[30] A. Arduino, A. Carena, and V. Curri, "Flexible FEC Optimization for Time-Domain Hybrid Modulation Formats," presented at *Advanced Photonics 2015*, Boston, USA, 2015, Paper SpM4E.4.

[31] K. Kojima, D. S. Millar, T. Koike-Akino, K. Parsons, S. Kametani and T. Sugihara, "Maximizing Transmission Capacity of Superchannels using Rate-Adaptive FEC," presented at *European Conference on Optical Communications*, Cannes, France, 2014, Paper P.3.23.

[32] A. Ghazisaeidi, L. Schmalen, I. F. J. Ruiz, P. Tran, C. Simonneau, P. Brindel, and G. Charlet, "Transoceanic Transmission Systems Using Adaptive Multirate FECs," *Journal of Lightwave Technology*, vol. 33, no. 7, pp. 1479–1487, 2015.

[33] A. Ghazisaeidi, I. F. J. Ruiz, L. Schmalen, P. Tran, C. Simonneau, E. Awwad, B. Uscumlic, P. Brindel, and G. Charlet, "Submarine Transmission Systems Using Digital Nonlinear Compensation and Adaptive Rate Forward Error Correction," *Journal of Lightwave Technology*, vol. 34, no. 8, pp. 1886–1895, 2016.

[34] A. Nespola, S. Straullu, A. Carena, G. Bosco, R. Cigliutti, V. Curri, P. Poggiolini, M. Hirano, Y. Yamamoto, T. Sasaki, J. Bauwelinck, K. Verheyen, and F. Forghieri, "GN-model Validation over Seven Fiber Types in Uncompensated PM-16QAM Nyquist-WDM Links," *Photonics Technology Letters*, vol. 26, no. 2, pp. 206–209, 2014.

[35] I. Fatadin, D. Ives and S. J. Savory, “Blind Equalization and Carrier Phase Recovery in a 16-QAM Optical Coherent System,” *Journal of Lightwave Technology*, vol. 27, no. 15, pp. 3042–3049, 2009.

[36] F. P. Guiomar, S. B. Amado, A. Carena, G. Bosco, A. Nespola, A. Teixeira, and A. N. Pinto, “Fully Blind Linear and Nonlinear Equalization for 100G PM-64QAM Optical Systems,” *Journal of Lightwave Technology*, vol. 33, no. 7, pp. 1265–1274, 2015.

[37] X. Zhou, “An Improved Feed-Forward Carrier Recovery Algorithm for Coherent Receivers With M-QAM Modulation Format,” *Photonics Technology Letters*, vol. 22, no. 14, pp. pp. 1051–1053, 2010.

[38] L. Du and J. L. Arthur, “The validity of "Odd and Even" channels for testing all-optical OFDM and Nyquist WDM long-haul fiber systems,” *Optics express*, vol. 20, no. 26, pp. B445–B451, 2012.

[39] R. Dar, et al. “Impact of WDM channel correlations on nonlinear transmission,” presented at *European Conference on Optical Communication*, 2016.

[40] F. P. Guiomar, and A. Carena, “Achieving Fine Bit-Rate Granularity with Hybrid Subcarrier Modulation,” presented at *Advanced Photonics*, Vancouver, Canada, July 18-20, 2016, Paper SpW3F.2.

[41] E. F. Mateo and G. Li, “Compensation of interchannel nonlinearities using enhanced coupled equations for digital backward propagation,” *Appl. Opt.*, vol. 48, no. 25, pp. F6–F10, 2009.